SCIENTIFIC REPORTS

OPEN

SUBJECT AREAS:
ELECTRONIC MATERIALS AND DEVICES
APPLIED PHYSICS
MATERIALS CHEMISTRY
ENGINEERING

Received
24 November 2011

Accepted
18 April 2012

Published
3 May 2012

Correspondence and requests for materials should be addressed to A.K. (kumatani@wpi-aimr.tohoku.ac.jp) or K.T. (TSUKAGOSHI.Kazuhito@nims.go.jp)

* Current address: WPI-Advanced Institute for Materials Research (WPI-AIMR), Tohoku University, Sendai 980-8578, Japan.

Solution-processed, Self-organized Organic Single Crystal Arrays with Controlled Crystal Orientation

Akichika Kumatani[1]*, Chuan Liu[1], Yun Li[1], Peter Darmawan[1], Kazuo Takimiya[2], Takeo Minari[1] & Kazuhito Tsukagoshi[1,3]

[1]WPI center for Materials Nanoarchitectronics (WPI-MANA), National Institute of Materials Science (NIMS), Tsukuba, Ibaraki 305-0044, Japan, [2]Department of Applied Chemistry, Graduate School of Engineering, Institute for Advanced Materials Research, Hiroshima University, Hiroshima 739-8524, Japan, [3]CREST-JST, Kawaguchi, Saitama 332-0012, Japan.

A facile solution process for the fabrication of organic single crystal semiconductor devices which meets the demand for low-cost and large-area fabrication of high performance electronic devices is demonstrated. In this paper, we develop a bottom-up method which enables direct formation of organic semiconductor single crystals at selected locations with desired orientations. Here oriented growth of one-dimensional organic crystals is achieved by using self-assembly of organic molecules as the driving force to align these crystals in patterned regions. Based upon the self-organized organic single crystals, we fabricate organic field effect transistor arrays which exhibit an average field-effect mobility of 1.1 $cm^2V^{-1}s^{-1}$. This method can be carried out under ambient atmosphere at room temperature, thus particularly promising for production of future plastic electronics.

The ongoing proliferation of electronic devices and growing concerns about increasing environmental burdens are leading to increasing demands for solution-based fabrication methods, which will contribute towards a sustainable society with their low carbon emissions. The use of soluble organic semiconductors enables fabrication of plastic electronic devices, such as organic field effect transistors (OFETs), organic light emitting diodes and organic solar cells, with both low cost and low energy consumption[1–3]. In particular, organic single crystals have been reported to exhibit high performance in OFETs because of the absence of grain boundaries and the resulting low defect density[4–16]. However, to integrate organic single crystals into practical devices as active materials two techniques must be developed. The first is the patterned growth of organic single crystals on desired regions, which is necessary for reducing the crosstalk among neighboring devices. For instance, Briseno *et al.* formed organic single crystal arrays on selective surface areas by exploiting the different surface properties of a pattern produced by a polydimethylsiloxane stamp, but these crystals were grown from the vapor phase[17]. Thereafter, several studies have been conducted on the formation and/or patterning of organic single crystals on a substrate by solution processes[18–35]. The second requirement is the ability to control the orientation of the organic crystals. Charge transport in organic crystals depends upon their orientation, due to their commonly having an anisotropic molecular arrangement[16], which can lead to considerable variability in the electrical performance of devices. Therefore, the ability to control both the position and orientation of deposited crystals is essential for practical application of organic crystals to devices. Recently, Minemawari *et al.* demonstrated an inkjet printing process for fabricating single crystal films with the organic semiconductor dioctylbenzothienobenzothiophene (C8-BTBT)[33]. They have used a technique combining antisolvent crystallization and inkjet printing, resulting in the formation of highly uniform organic single crystal films at the desired locations, and OFETs with an extremely high average mobility of 16.4 $cm^2V^{-1}s^{-1}$. In this method, crystal nucleation occurs due to the evaporation of solvent.

In this work, we develop a bottom-up method which enables aligned formation of organic single crystals on a substrate by self-assembly. The use of self-assembly as a driving force to form a mono-crystalline semiconductor layer is particularly promising for printable electronics technology, because it can be performed under ambient atmosphere at room temperature. Here we use C8-BTBT as the organic semiconductor, which tends to form one-dimensional crystal under solvent vapor. Our method is based upon the confinement effect induced by different surface wettabilities, where the organic crystals are grown in the narrow trenches to restrict the growth direction.

Consequently, we develop a process for the direct formation of organic single crystals using a self-organised solution-based method with both their position and orientation being controlled. The spontaneous alignment of one-dimensional crystals is possible not only for organic semiconductors[18,27] but also for some inorganic materials[36–38], as long as the materials can create one-dimensional single crystal structure. We also demonstrate that this method can fabricate organic FETs. The devices exhibit an average field-effect mobility (μ_{FET}) of 1.1 $cm^2V^{-1}s^{-1}$. The simplicity of the proposed method makes it a promising candidate for widespread adoption in future electronics based on single crystals.

Results

Fabrication of organic single crystal arrays by self-organization with controlled crystal direction. In order to realize oriented growth of organic crystals, we employed polymer assisted solvent vapor annealing (PASVA)[32,34]. C8-BTBT was used as the organic semiconductor material because as it has been shown to be a good candidate for creating one-dimensional rod-like structures with good air-stability and a high device mobility[32,34,39]. The PASVA offers the advantage of being an all-solution process that can produce high-quality organic single crystals at room temperature. In a previous report, we demonstrate the direct formation of C8-BTBT single crystals on a polymer base film under solvent vapor[32]. This process relies on the solubility of the polymer base film, which allows semiconductor molecules to travel significant distances on the surface. Consequently, PASVA enables the reorganisation of molecules into single crystals with lengths of up to several hundred micrometers. C8-BTBT tends to form long rod-like crystals, the long axis of which corresponds to the [100] crystal direction. This method was carried out on a patterned substrate, limiting the growth direction of the crystals and allowing fine control of the crystal location and orientation over a wide area.

We first patterned the substrate surface into regions that were either wettable or unwettable by the organic semiconductor solution[29–31,35]. A silicon wafer with a 200-nm-thick silicon dioxide layer was used as the substrate. The solution-wettable surface regions were first produced by UV-ozone cleaning. As illustrated in Figure 1a, a photoresist pattern was formed by photolithography on the wettable surface. A fluoropolymer, CytopTM, was then spin-coated and annealed for 2 hours at 90°C. The photoresist was subsequently lifted off to form unwettable Cytop regions on the substrate enclosing a pattern of wettable trenches. At this stage, the thickness of the Cytop layer measured by a surface profilometer was approximately 100 nm. An anisole solution of C8-BTBT (1 wt%) and poly(methylmethacrylate) (PMMA, 2 wt%) was then applied to the substrate, resulting in trace amounts of the semiconductor solution entering the wettable trenches. As the anisole evaporated, a polycrystalline C8-BTBT film was formed on an underlying PMMA film by vertical phase separation (similar to that reported in Ref.[29]) exclusively in the trenches. The PASVA with chloroform was then carried out for 10 hours, causing the polycrystalline C8-BTBT films in the trenches to recrystallize into rod-like single crystals oriented along the trench directions. As shown in a cross section in Figure 1b, the typical thicknesses of the crystals and PMMA layers were 250 nm and 80 nm, respectively. Besides, without PMMA the crystals were not grown in the trenches, with the role of PMMA being to absorb the chloroform solvent, enabling C8-BTBT molecules to move easily for crystallization.

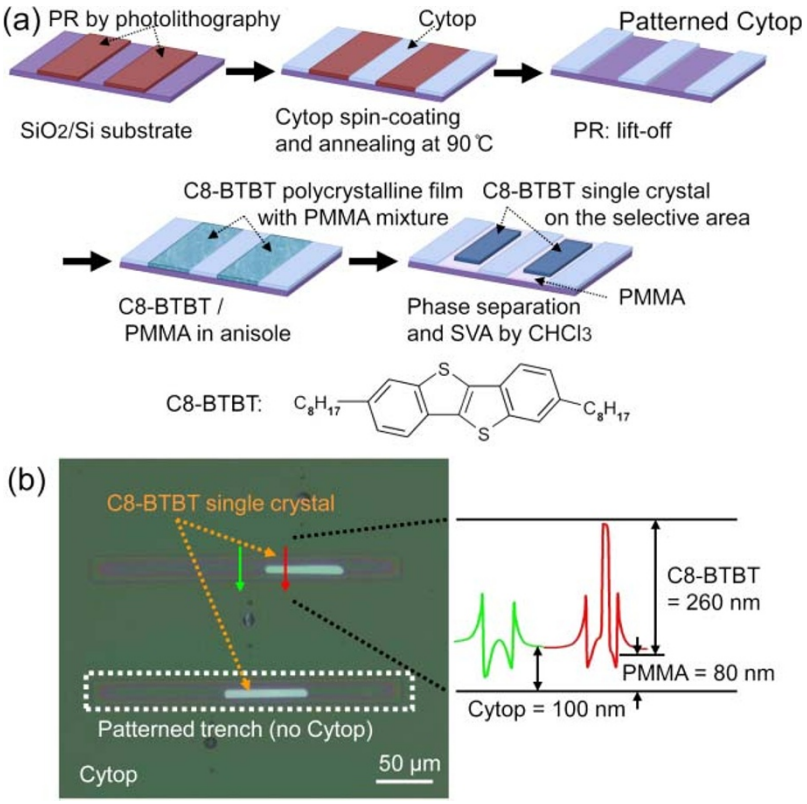

Figure 1 | Organic single crystal arrays on the patterned Cytop substrate. (a) Schematic outline of the fabrication of self-aligned organic single crystal arrays. The wettable trenches are formed by patterning an anisole-unwettable 100-nm-thick Cytop layer using a standard photolithographic technique. A solution of C8-BTBT/PMMA in anisole is applied but remains only in the wettable trenches, because the surrounding Cytop region repels it. During PASVA with chloroform, the C8-BTBT film becomes recrystallized into single crystal arrays with the same orientation. The insert is the molecular structure of C8-BTBT. (b) Organic single crystals fabricated by the present method. The polarized optical micrograph shows the crystals are fabricated only in the trenches and have the same crystal orientation. The surface profile shows that the typical thickness of the crystals is about 250 nm.

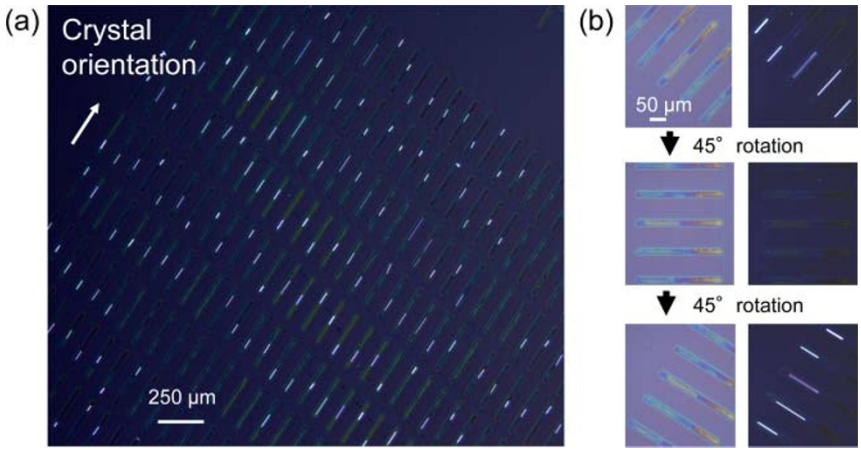

Figure 2 | Organic single crystal arrays with controlled crystal orientation in large scale. (a) Polarized optical micrograph of an organic single crystal array. (b) Optical micrographs of crystals with and without a polarizer. The polarized images show the diagonal and extinction positions of the crystals. The images were taken at the positions rotated 45° for each with the diagonal and extinction positions.

Thus, by patterning wettable areas on the surface and using PASVA, we successfully form an organic single crystal array with a single crystal orientation over a wide area. A polarized optical micrograph of the array is shown in Figure 2a. It can be clearly seen that the crystals are formed only in the trenches and that they have a similar color and brightness. This indicates that the technique allows good control of both the crystal position and orientation. An analysis of the optical micrographs showed that 83% of the 270 trenches were occupied by crystals, 98% of which were preferentially aligned with a certain crystal orientation. The remaining 17 % of empty trenches without C8-BTBT single crystals in the figure were likely caused by uncompleted crystal creation due to the lack of either PMMA or C8-BTBT molecules. Figure 2b shows polarized optical micrographs of crystals rotated 45° between each image with the diagonal and extinction positions. This observation confirms that the crystals have the same orientation as the patterned trenches. We also perform X-ray diffraction analysis of these aligned crystals to investigate their internal crystallinity, as shown in Supplementary information 1. From the diffraction signals obtained, it can be confirmed that the C8-BTBT molecules are stacked in the same direction [100] as we reported previously[32,34]. Thus, it implies that the rod-like structure of crystals aligned is coincident with crystals in Ref.[32]. Consequently, polarized optical microscopic images and X-ray diffraction patterns suggest that the all the crystals are aligned with the same crystal orientation.

Discussions

Since crystal alignment occurs during the PASVA process, we investigate the mechanism of oriented crystal growth in order to determine which parameters have the largest influence on crystal alignment. We first consider the effect of substrate orientation during PASVA. Figure a) in Supplementary information 2 shows aligned crystals in two perpendicular trenches formed on a tilted substrate. It can be seen that the crystals grew equally well within both trenches, indicating no dependence on substrate orientation. We suspect that within each trench the underlying PMMA is not completely melted, rather they gather together expelling C8-BTBT, independently of substrate tilt. Similar results are found for a tilted substrate having eight trenches along different directions (Figure b) in Supplementary information 2). Here, the polarized micrographs clearly indicate that the crystal orientation is determined only by the trench direction, and the substrate orientation does not have any effect.

To gain yet more information on the crystal alignment mechanism, we observe the crystal growth process during PASVA using real-time video. As shown in Figure 3, the crystal gradually orients itself along the trench direction as it grows longer. As the C8-BTBT crystal starts crystallizing (t = 0), the crystal is almost aligned perpendicular to the trench direction. As time advances, the ends of the crystal reach the sides of the trench, and then start to change the growth direction along the long axis of the trench. Thus, the PASVA process causes strong alignment of the crystal along the trench direction. Also, we consider the affinity between molecule-molecule and molecule-substrate. As we have reported in our previous work[32], a C8-BTBT and PMMA mixture is at first spin-coated on the patterned substrate and exists as a phase separated film. After it is dried, PASVA is applied using a chloroform vapor. During PASVA, both C8-BTBT and PMMA are dissolved by the vapor in a liquid-like phase. Due to the differential solubility in chloroform, PMMA stacks together, expelling C8-BTBT, and consequently inducing C8-BTBT crystallization on the PMMA surface as rod-like structures. Therefore, the C8-BTBT itself is not affected by the substrate, forming crystals with the (100) crystal orientation, independently of any substrate interaction. Proof that PMMA exists underneath crystals is confirmed by capacitance-voltage measurements as shown in the section of field effect transistors and also in Ref.[32]. Thus, the major driving force for the change in crystal orientation is clearly the self-assembling ability of C8-BTBT molecules toward a [100] crystal

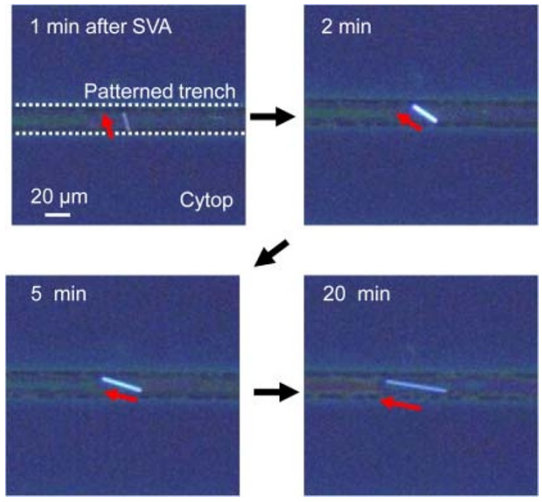

Figure 3 | Real-time observation of the crystal growth and alignment process. The polarized optical micrographs were taken at 1, 2, 5, and 20 min after the start of the PASVA process. The red-arrows are guides showing the [100] crystal orientation.

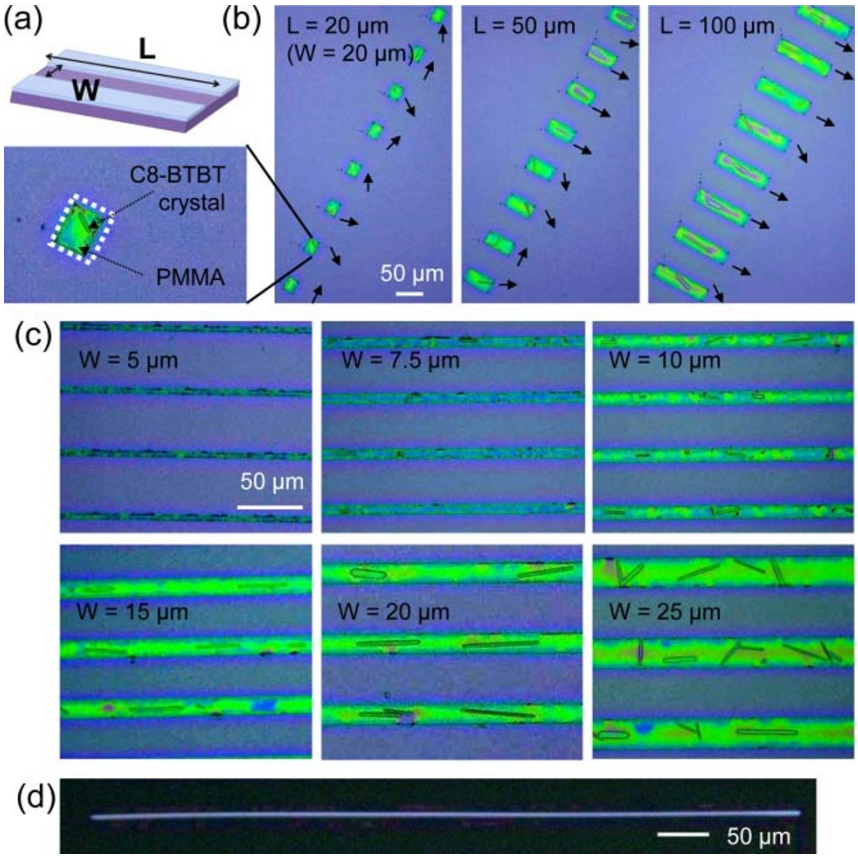

Figure 4 | Control of the crystal orientation by trench size on the substrate. (a) Schematic diagram of the trench geometry defined by the length (L) and width (d). (b) Optical micrographs of samples after crystal growth for different L and a fixed W of 20 μm. The black arrows indicate the [100] direction of the C8-BTBT crystals. (c) Optical micrographs of samples with the different W and sufficiently large L. (d) Polarized optical micrograph of the longest crystal obtained. The length of the crystal was 685 μm.

orientation, which is preferred for C8-BTBT molecular stacking. When the crystal is about to grow longer than the trench width due to the strong interaction among molecules, it is forced to align along the trench direction due to the unwettability of C8-BTBT on Cytop. Another important factor is the solubility in chloroform vapor of the PMMA layer underneath the crystals. During PASVA, the PMMA surface may melt and swell in the solvent vapor, which decreases the interaction between the organic semiconductor and the underlying polymer film, increasing the molecular mobility on the surface, resulting in the self-aligned formation of oriented crystals in the patterned trenches.

We also investigate the effect of trench geometry on the crystal formation process. Figure 4 shows optical micrographs of crystals formed by PASVA trenches of different lengths (L) and widths (W). All other fabrication conditions, such as the volume of organic semiconductor solution used and the annealing time, are exactly the same for all samples. We first examine crystal formation in trenches with different L and fixed W (= 20 μm). As can be seen in Figure 4b, the crystal orientation is found to clearly depend on the trench geometry. For the case of a square trench (L = W = 20 μm), the crystal orientation is random. On the other hand, crystals tend to align along the long direction of the trench as L increases, which suggests that the trenches must be longer in one direction to effectively align crystals. We next examine the effect of varying W for sufficiently large L (Figure 4c). For W = 5 μm, no crystallization of C8-BTBT is found to occur in the trench, probably due to an insufficient amount of C8-BTBT and underlying PMMA in such a narrow trench or the unwetting PMMA of in the very narrow trench. A slight improvement in the crystallization degree is observed for the samples with W = 7.5–10 μm. Some crystals are formed but they are too small to become aligned in the trench. For W = 15–20 μm, sufficiently large crystals are formed with a relatively small spread in orientation. The crystals are typically longer than 50 μm, with the largest being longer than 600 μm (Figure 4d). However, for W > 25 μm, the spread in orientations tends to increase, probably due to insufficient confinement within the trench. Consequently, a W value of around 20 μm can be considered to be the most appropriate for optimizing the degree of crystal orientation. In organic materials, C8-BTBT is one of the most promising candidates for this method for device application. However, we are confident that a controlled growth direction of other organic solution-processable single crystals such as BTBT derivatives, perylene-bis(dicarboximide) derivatives or trimethylsilane-aquarterthiophene is possible[18,27]. In the case of other materials, the trench size and width need to be optimized.

We next fabricate OFETs using the aligned single crystals fabricated by this method. The OFETs are fabricated with a bottom-gate top-contact structure as shown in Figure 5a. A highly doped Si substrate is used as a gate electrode, and the silicon dioxide and PMMA layers underneath the organic crystals act as a gate insulator. The long axis direction of the crystals corresponds to the [100] crystal orientation along which the largest π-orbital overlap among neighboring molecules is expected[40]. Since the highest occupied molecular orbital (HOMO) of C8-BTBT is known to be 5.7 eV, and a relatively large charge injection barrier is expected for gold source/drain electrodes, an amorphous iron (III) chloride ($FeCl_3$) layer is inserted at the metal/organic interface. $FeCl_3$ is known as a strong acceptor, which improves the charge injection efficiency. The charge injection barrier between the HOMO of C8-BTBT and Au is reduced by the acceptors, thereby inducing charge transfer between C8-BTBT and $FeCl_3$[41,42]. Using this $FeCl_3$/Au electrode configuration, 32 OFET

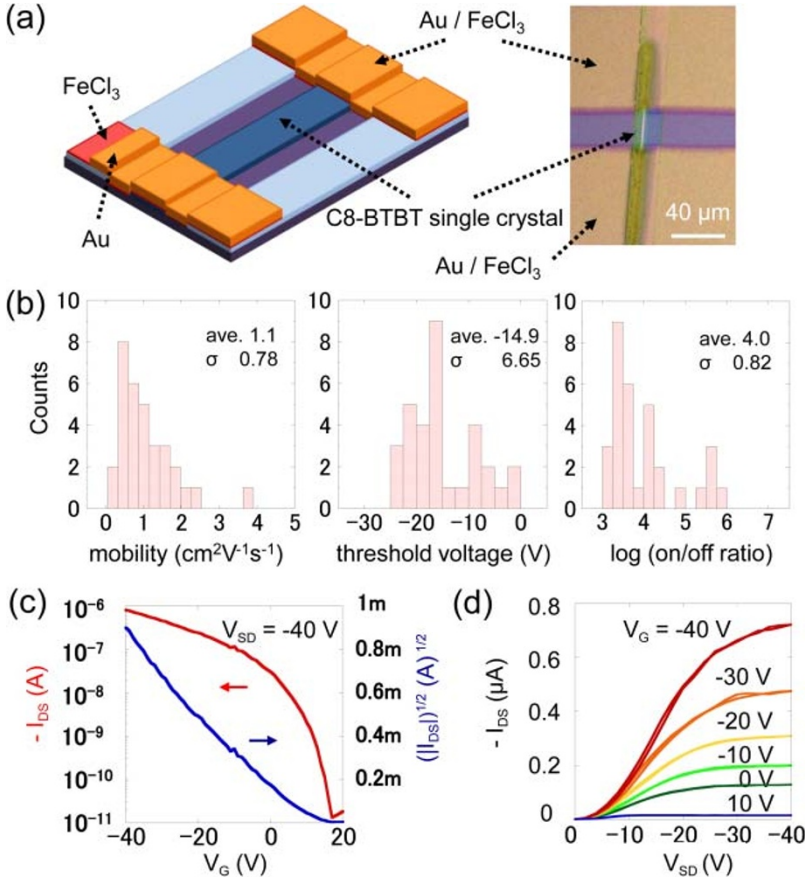

Figure 5 | Organic single crystal field effect transistors. (a) A schematic diagram of the device structure and optical microscopic image of the transistor. (b) Histograms of field effect mobility: 1.1 $cm^2V^{-1}s^{-1}$ (standard deviation: 0.78 and maximum mobility: 3.8 $cm^2V^{-1}s^{-1}$), threshold voltage: −14.9 V (σ: 6.65) and log (on/off ratio) 4.0 (σ:0.82) measured 32 transistors. (b) Transfer and (c) output characteristics of a typical device.

devices are fabricated. Values of field effect mobility, threshold voltage and on/off ratio are extracted for the all devices fabricated and their distribution is shown in Figure 5b. Also, typical transfer and output characteristics of the devices are shown in Figure 5c and d, respectively. An average value of the mobility of 1.1 $cm^2V^{-1}s^{-1}$ (standard deviation: 0.78 and maximum mobility: 3.8 $cm^2V^{-1}s^{-1}$) is obtained. The mobility value is lower than our previous report[32] and a recently published report by Minemawari et al.[33] This would be due to the relatively short channel length used (35 μm) and the large contact resistance. The effect of the contact resistance can be seen in the output characteristics (Fig. 5d), where the drain current increases nonlinearly at the low drain voltage region. The large contact resistance is probably induced by the energy level mismatch between Fermi level of Au and HOMO of C8-BTBT or relatively large thickness of the crystals[32], although we insert the acceptor layer to suppress these unfavorable effects. On the other hand, the devices show ideal transistor behavior in the transfer characteristics (Fig, 5c) with an average on/off ratio of 10^4, indicating a possibility to use our method for practical fabrication process in plastic electronics. Furthermore, the performance distribution exhibited is similarly narrow, as reported by organic field effect transistors, in terms of standard deviation[32,33,35]. The simplicity of this method can be applied to other solution processable materials having an one-dimensional structure such as solution-processable zinc oxide[36,37] and lanthanide hydroxide nanorods[38]. Thus, this method is suitable to be used for the fabrication of single crystal arrays and provides a new solution-processing method to control the orientation of single crystals in many fields.

In conclusion, we develop a solution-based method for the fabrication of organic single crystal arrays with controlled crystal orientation using PASVA in confined areas on the surface. We demonstrate that C8-BTBT crystals can be self-organized in patterned wettable rectangular regions on a substrate, and that the [100] crystal direction can be aligned along the long axis of the rectangle. The driving force is found to be the self-assembling ability of the C8-BTBT molecules on the soluble polymer base film. The influence of the geometry of the confinement area on the crystal alignment is also discussed. Moreover, OFETs based on the aligned crystals are demonstrated with an average field-effect mobility of 1.1 $cm^2V^{-1}s^{-1}$ measured across 32 devices. These results indicate that the proposed technique is promising for future large-area electronics based upon all solution-processable single crystals.

Methods

Patterned Cytop Substrate. All experiments were carried out under ambient conditions. A highly doped n-type [100] silicon wafer with a 200-nm-thick SiO_2 layer was used as a substrate. The wafer was cleaned with solvents and treated with ultraviolet (UV) ozone to make the surface wettable for organic solutions. Photoresist (PR, ma-N 1400, micro resist technology, Germany) was spin-coated on the substrate and patterned by a typical photolithographic technique. Cytop™ (Asahi Glass, Japan) was diluted with the developer (CT-Solv. 180) at a ratio of 1:2 and spin-coated onto the PR patterned substrate. The substrate was annealed at 90°C for two hours. The PR was then lifted off, resulting in a patterned Cytop layer on the substrate. The thickness of the Cytop layer was measured to be about 100 nm using a surface profiler.

C8-BTBT Solution. C8-BTBT (Nippon Kayaku) and PMMA (Nippon Zeon, M_W = 950,000) were dissolved in anisole (1 wt.% for C8-BTBT and 2 wt% for PMMA).

Aligned Crystal Growth. The C8-BTBT solution was applied to the patterned substrate, but remained only in the trenches due to their wettability, and PASVA was performed with chloroform vapor for 10 hours. The growth process is similar to the process described in Ref.[32]. Optical images, including the real-time images of the self-alignment process in Figure 3, were obtained using a digital optical microscope (VHX-1000, Keyence).

FET Fabrication and Characterization. OFETs were fabricated using the aligned crystals with the [100] crystal direction corresponding to the channel direction. Source and drain electrodes were thermally evaporated at a rate of 0.1 Å/s for $FeCl_3$ (0.3 nm) and gold (40 nm) through a metal shadow mask in vacuum (under 5×10^{-4} Pa). The OFET characteristics were measured in vacuum (under 5×10^{-4} Pa) using an Agilent 4156C parameter analyzer. *Ci* (capacitance per unit area) measured by capacitance-voltage measurement is about 30 $nFcm^{-2}$ at 50 Hz.

1. Sirringhaus, H. Device Physics of Solution-Processed Organic Field-Effect Transistors. *Adv. Mater.* **17**, 2411 (2005).
2. Xiao, L. *et al.* Recent Progresses on Materials for Electrophosphorescent Organic Light-Emitting Devices. *Adv. Mater.* **23**, 926 (2011).
3. Brabec, C. J. *et al.* Solution-Processed Organic Solar Cells. *MRS Bull.* **33**, 670 (2008).
4. Virkar, A. A. *et al.* Organic Semiconductor Growth and Morphology Considerations for Organic Thin-Film Transistors. *Adv. Mater.*, **22**, 3857 (2010)
5. Fichou, D. S. *et al.* First evidence of stimulated emission from a monolithic organic single crystal: octithiophene.. *Adv. Mater.* **9**, 1178 (1997).
6. de Boer, R. W. I. *et al.* Organic Single-Crystal Field-Effect Transistors. *Phys. Stat. Soli. A.* **201**, 1302 (2004).
7. Saunder, V. C. *et al.* Elastomeric Transistor Stamps: Reversible Probing of Charge Transport in Organic Crystals. *Science* **303**, 1644 (2004).
8. Jurchescu, O. D. *et al.* Effect of impurities on the mobility of single crystal pentacene. *Appl. Phys. Lett.* **84**, 3061 (2004).
9. Stassen, A. F. *et al.* High charge carrier densities and conductance maxima in single-crystal organic field-effect transistors with a polymer electrolyte gate dielectric. *Appl. Phys. Lett.* **85**, 3899 (2004).
10. Gershenson, M. E. *et al.* Colloquium: Electronic Transport in Single-Crystal Organic Transistors. *Rev. Mod. Phys.* **78**, 973 (2006).
11. Takeya, J. *et al.* In-Crystal and Surface Charge Transport of Electric-Field-Induced Carriers in Organic Single-Crystal Semiconductors. *Phys. Rev. Lett.* **98**, 196804 (2007).
12. Hulea, I. N. *et al.* Tunable Fröhlich polarons in organic single-crystal transistors. *Nature Mater.* **5**, 982 (2006).
13. Goldmann, C. *et al.* Hole mobility in organic single crystals measured by a "flip-crystal" field-effect technique. *J. Appl. Phys.* **96**. 2080 (2004).
14. Cornil, J. *et al.* Electronic Structure of the Pentacene Single Crystal: Relation to Transport Properties. *J. Am. Chem. Soc.* **123**, 1250 (2001).
15. Lee, J. Y. *et al.* Anisotropic field effect mobility in single crystal pentacene. *Appl. Phys. Lett.* **88**, 252106 (2006)
16. Podzorov, V. *et al.* Intrinsic charge transport on the surface of organic semiconductors. *Phys. Rev. Lett.* **93**, 086602 (2004).
17. Briseno, A. L. *et al.* Patterning organic single-crystal transistor arrays. *Nature* **444**, 913 (2006).
18. Mannsfield, S. C. B. *et al.* Highly Efficient Patterning of Organic Single-Crystal Transistors from the Solution Phase. *Adv. Mater.* **20**, 4044 (2008).
19. Roberts, M. E. *et al.* Flexible, plastic transistor-based chemical sensors. *Org. Electron.* **10**. 377 (2009).
20. Reeze, C. & Bao, Z. Organic single-crystal field-effect transistors. *Materials Today* **10**, 20 (2007).
21. Uemura, T. *et al.* Very High Mobility in Solution-Processed Organic Thin-Film Transistors of Highly Ordered [1]Benzothieno[3,2-b]benzothiophene Derivatives. *Appl. Phys. Express* **2**, 111501 (2009).
22. Nakayama, K. *et al.* Patternable Solution-Crystallized Organic Transistors with High Charge Carrier Mobility. *Adv. Mater.* **23**, 1626 (2011).
23. Kim, D. H. *et al.* High-Mobility Organic Transistors Based on Single-Crystalline Microribbons of Triisopropylsilylethynyl Pentacene via Solution-Phase Self-Assembly. *Adv. Mater.* **19**, 678 (2007).
24. Lim, J. A. *et al.* Control of the Morphology and Structural Development of Solution-Processed Functionalized Acenes for High-Performance Organic Transistors. *Adv. Funct. Mater.* **19**, 1515 (2009).
25. Yamao, T. *et al.* Direct Formation of Thin Single Crystals of Organic Semiconductors onto a Substrate. *Chem. Mater.* **19**, 3748 (2007).
26. Zhou, Y. *et al.* High-Performance Organic Field-Effect Transistors from Organic Single-Crystal Microribbons Formed by a Solution Process. *Adv. Mater.* **22**, 1484 (2010).
27. Luca, G. D. *et al.* Non-conventional processing and post-processing methods for the nanostructuring of conjugated materials for organic electronics. *Adv. Funct. Mater.* **21**, 1279 (2011).
28. Minari, T. *et al.* Selective organization of solution-processed organic field-effect transistors. *Appl. Phys. Lett.* **92**, 173301 (2008).
29. Minari, T. *et al.* Surface selective deposition of molecular semiconductors for solution-based integration of organic field-effect transistors. *Appl. Phys. Lett.* **94**, 093307 (2009).
30. Kano, M. *et al.* Improvement of subthreshold current transport by contact interface modification in p-type organic field-effect transistors. *Appl. Phys. Lett.* **94**, 143304 (2009).
31. Kano, M. *et al.* All-Solution-Processed Selective Assembly of Flexible Organic Field-Effect Transistor Arrays. *Appl. Phys. Express* **3**, 051601 (2010).
32. Liu, C. *et al.* Solution-Processable Organic Single Crystals with Bandlike Transport in Field-Effect Transistors. *Adv. Mater.* **23**, 523 (2010).
33. Minemawari, H. *et al.* Inkjet printing of single-crystal films. *Nature.* **475**, 364 (2011).
34. Liu, C. *et al.* Direct formation of organic semiconducting single crystals by solvent vapor annealing on a polymer base film. *J. Mater. Chem.* **22**, 8462 (2012).
35. Li, Y. *et al.* Patterning solution-processed organic single crystal transistors with high device performance. *AIP in Advance* **1**, 022149 (2011).
36. Liu, B & Zeng, H. C. Hydrothermal Synthesis of ZnO Nanorods in the Diameter Regime of 50 nm. *J. Am. Chem. Soc.* **125**, 4430, 2007.
37. Liu, B & Zeng, H. C. Room Temperature Solution Synthesis of Monodispersed Single-Crystalline ZnO Nanorods and Derived Hierarchical Nanostructures. *Langmuir* **20**, 4196 (2004).
38. Wang, X & Li, Y. Synthesis and Characterization of Lanthanide Hydroxide Single-Crystal Nanowires. *Angew. Chem. Int. Ed.* **41**, 4790 (2002).
39. Ebata, H. *et al.* Highly Soluble [1]Benzothieno[3,2-b]benzothiophene (BTBT) Derivatives for High-Performance, Solution-Processed Organic Field-Effect Transistors. *J. Am. Chem. Soc.* **129**, 15732 (2007).
40. Izawa, T. *et al.* Molecular Ordering of High-Performance Soluble Molecular Semiconductors and Re-evaluation of Their Field-Effect Transistor Characteristics. *Adv. Mater.* **20**, 3388 (2008).
41. Minari, T. *et al.* Highly enhanced charge injection in thienoacene-based organic field-effect transistors with chemically doped contact. *Appl. Phys. Lett.* **100**, 093309 (2012).
42. Miyata, Y. *et al.* High-Performance Organic Field-Effect Transistors Based on Dihexyl-Substituted Dibenzo[d,d']thieno[3,2-b;4,5-b']dithiophene. *Jour. of Mater. Chem.* **22**, 8462 (2012).

Acknowledgements

We would like to thank Mr. Kuwabara, Dr. Ikeda, and Mr. Kanoh (Nippon Kayaku Co.) for providing the C8-BTBT. Authors acknowledge to Dr. James Stott in University College London and London Centre for Nanotechnology (UK) for fruitful discussion. This study is supported partially by the Grand-In-Aid for Scientific Research (Nos. 17069004, 21241038 and 21750197) from the Ministry of Education, Culture, Sport, Science and Technology of Japan.

Authors contributions

A.K. and K. T. designed research; A.K. performed most of experiments and wrote the manuscript. All authors planned and analysed the experimental results.

Additional information

Supplementary information accompanies this paper at http://www.nature.com/scientificreports

Competing financial interests: The authors declare no competing financial interests.

How to cite this article: Kumatani, A. *et al.* Solution-processed, Self-organized Organic Single Crystal Arrays with Controlled Crystal Orientation. *Sci. Rep.* **2**, 393; DOI:10.1038/srep00393 (2012).